FIGURE 2.1

Couette flow between two parallel plates at different temperatures. The top wall moves at a constant speed to the right.

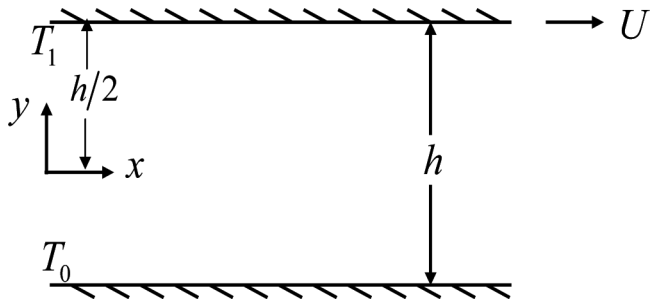

FIGURE 2.2

Combined Couette–Poiseuille flow driven by shear and non-dimensional pressure gradient, $P_0 = \frac{H^2}{2\mu U_2}(\rho X_x - F)$, with U_2 as the speed of the top wall; $F(t)$ is the time-dependent streamwise pressure gradient; X_x is the body force and **H** is the distance between the plates.

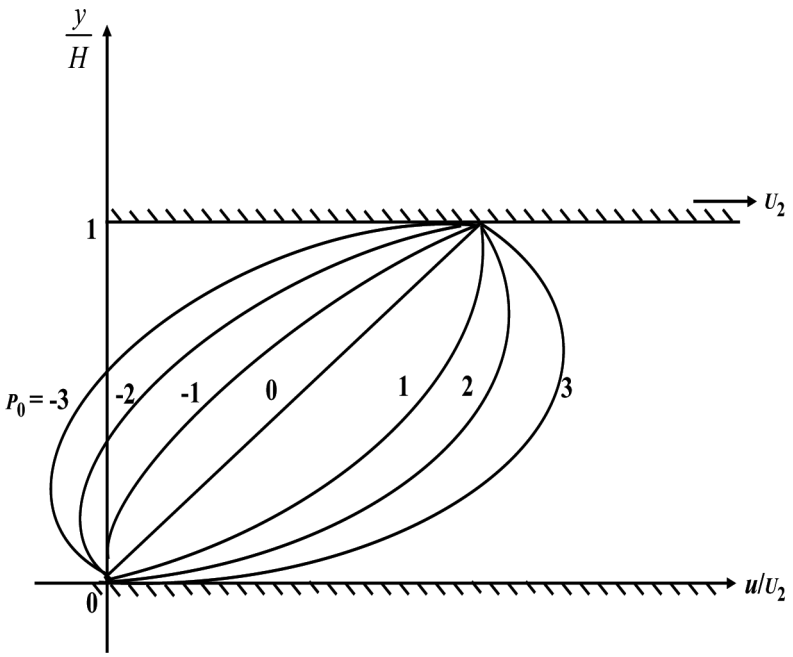

FIGURE 2.3

Streamlines sketched for the stagnation point flow, with the stagnation point at the origin.

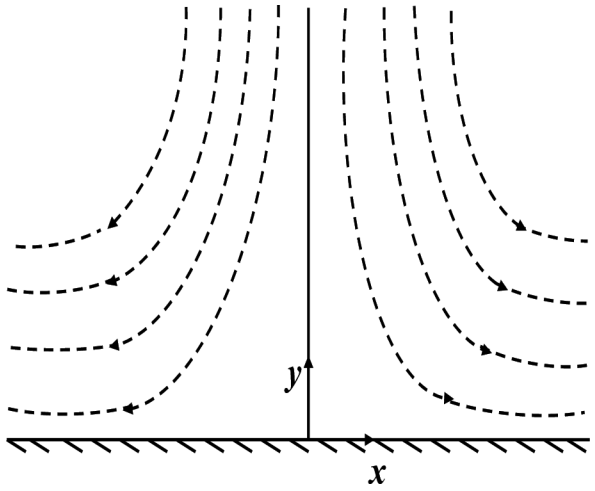

FIGURE 2.4

Solution of stagnation point flow, shown in the transformed η coordinate. Various quantities are as described in the text.

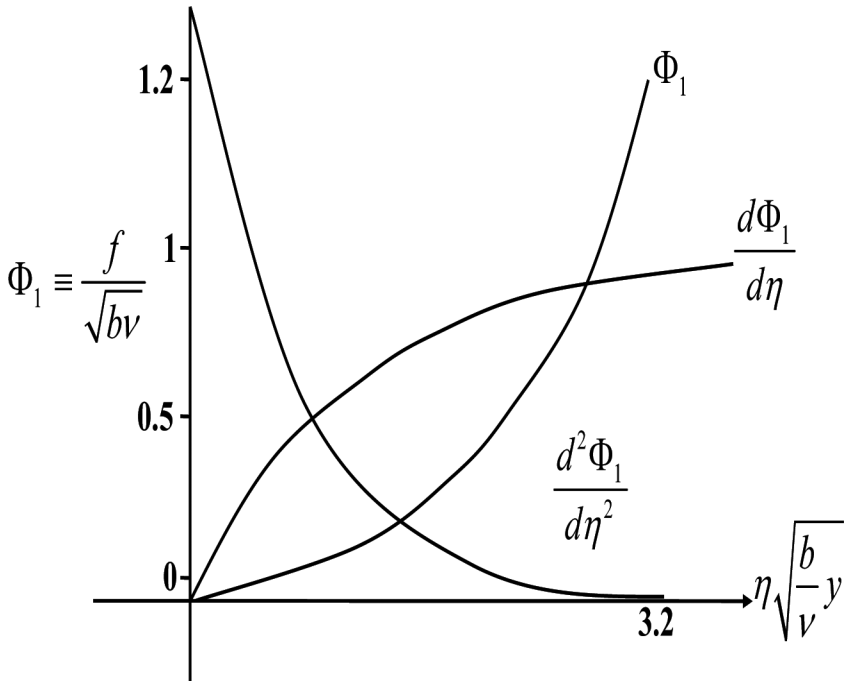

FIGURE 2.5

(a) Velocity profiles and (b) streamlines for the axisymmetric flow configuration.

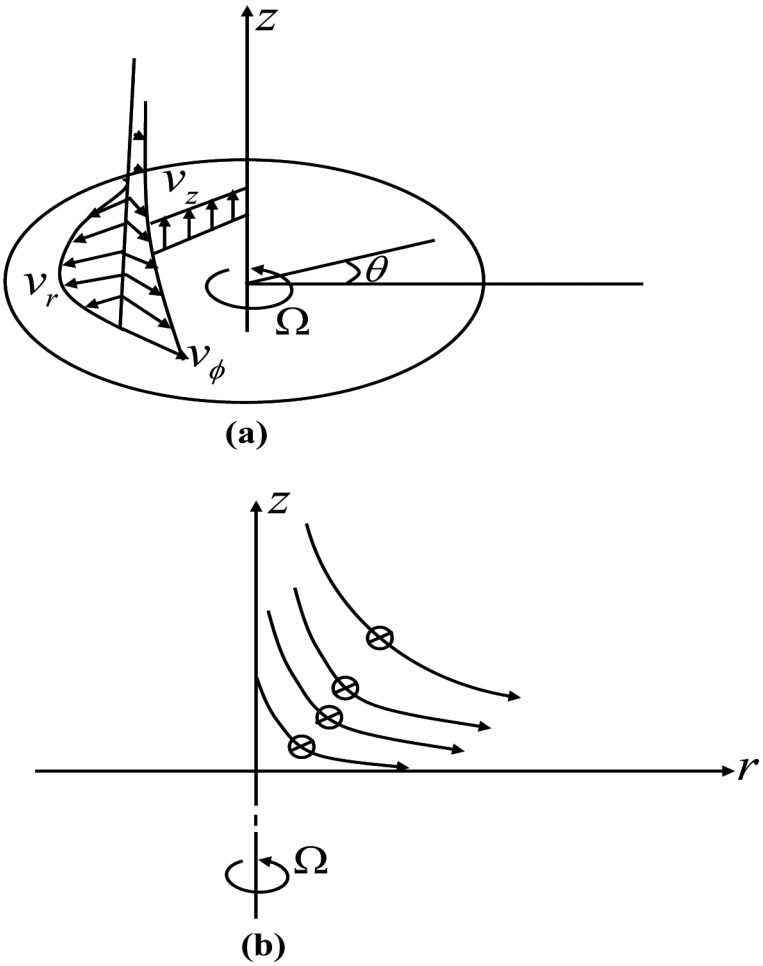

FIGURE 2.6

Solution components (as defined in the text) for the solution of Eqs. (2.94) to (2.97), with G^* as the tangential, $-f^*$ as the axial and g^* as the radial components of induced equilibrium flow.

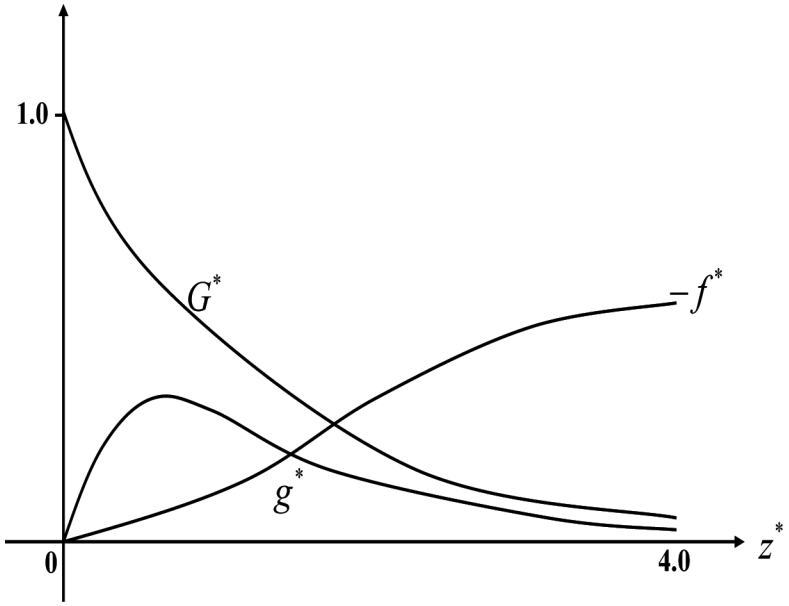

FIGURE 2.7

Control volume for flow past a plate to show the displacement effect. Note that the top segment is a streamline.

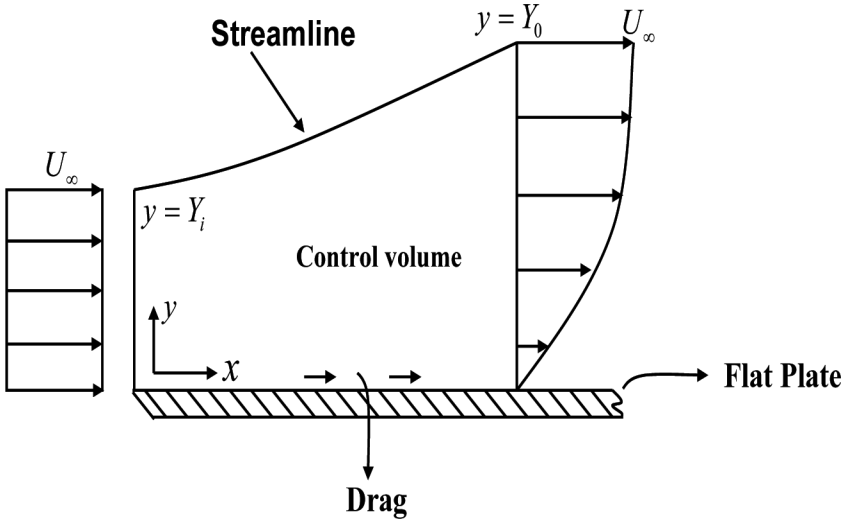

FIGURE 2.8

Velocity, shear and second derivative profile for an accelerated flow.

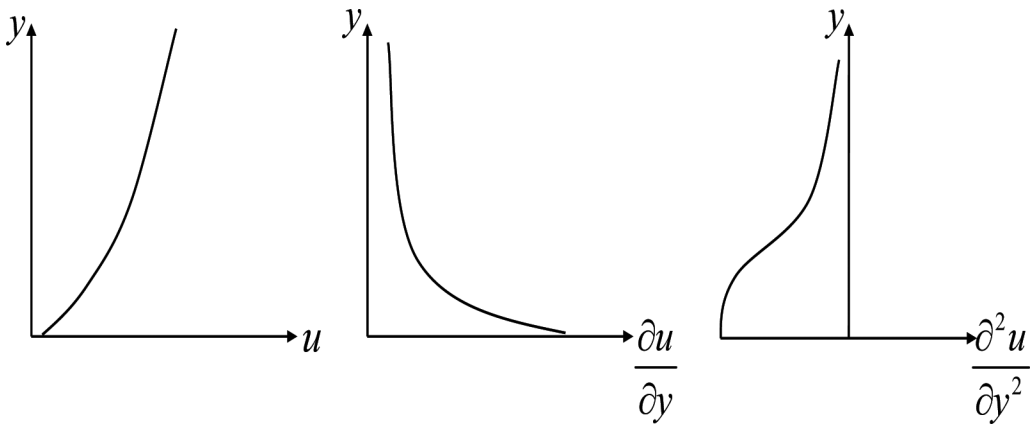

FIGURE 2.9

Velocity, shear and second derivative profile for a retarded flow with the point of inflection marked.

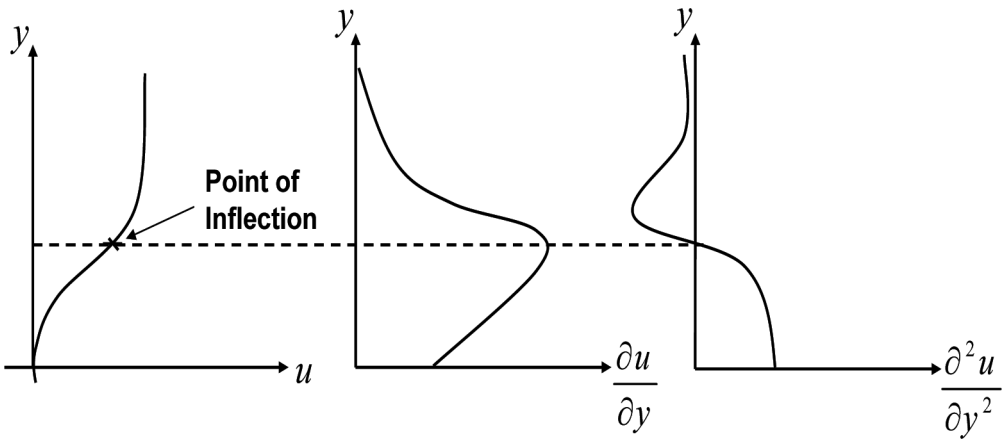

FIGURE 2.10

Sketch of a velocity profile under the influence of an adverse pressure gradient, with S as the point of separation, for steady flow ($\tau_w = 0$). On the bottom are shown the streamlines.

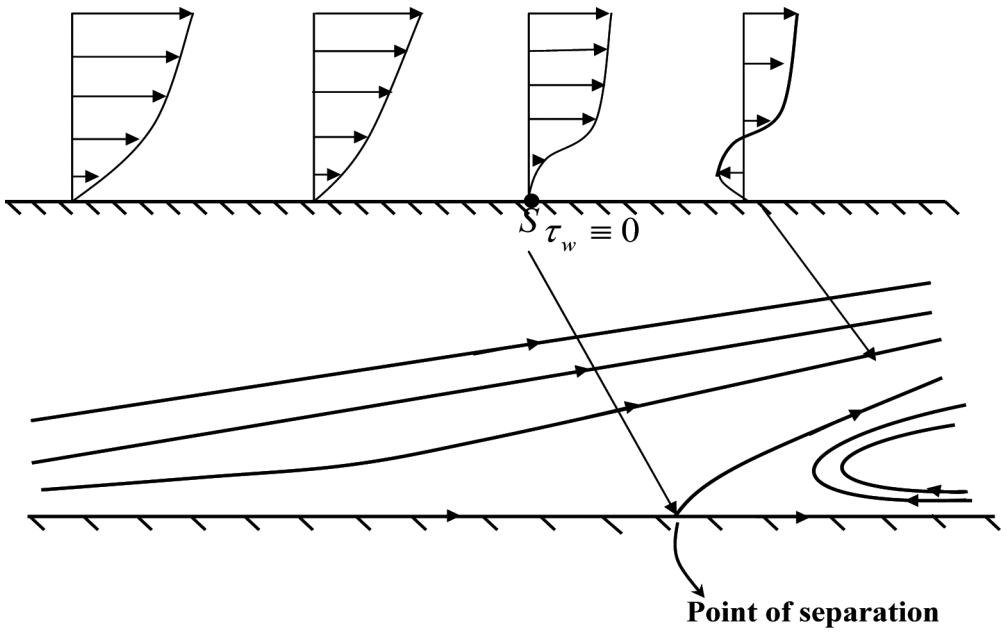

FIGURE 2.11

Formation of a laminar mixing layer starting from two uniform flows with velocity U_1 and U_2, shown on the left.

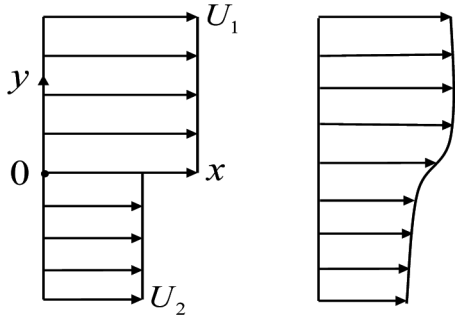

FIGURE 2.12

A typical energy spectrum of a two-dimensional flow over a flat plate. Note that the spectrum varies as k^{-3} for an intermediate wavenumber range [323].

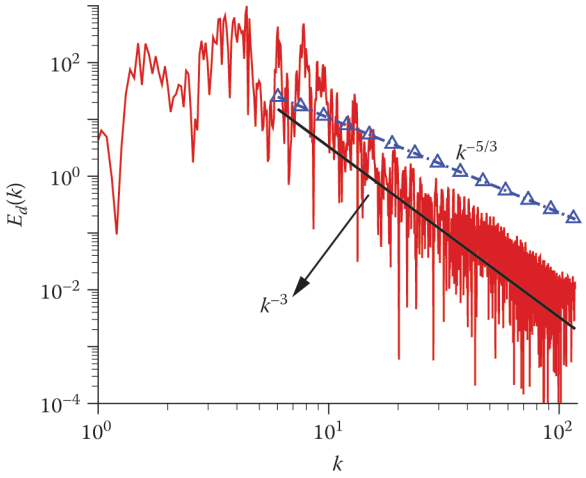

FIGURE 2.13

Phenomenon of modulation in a group of waves.

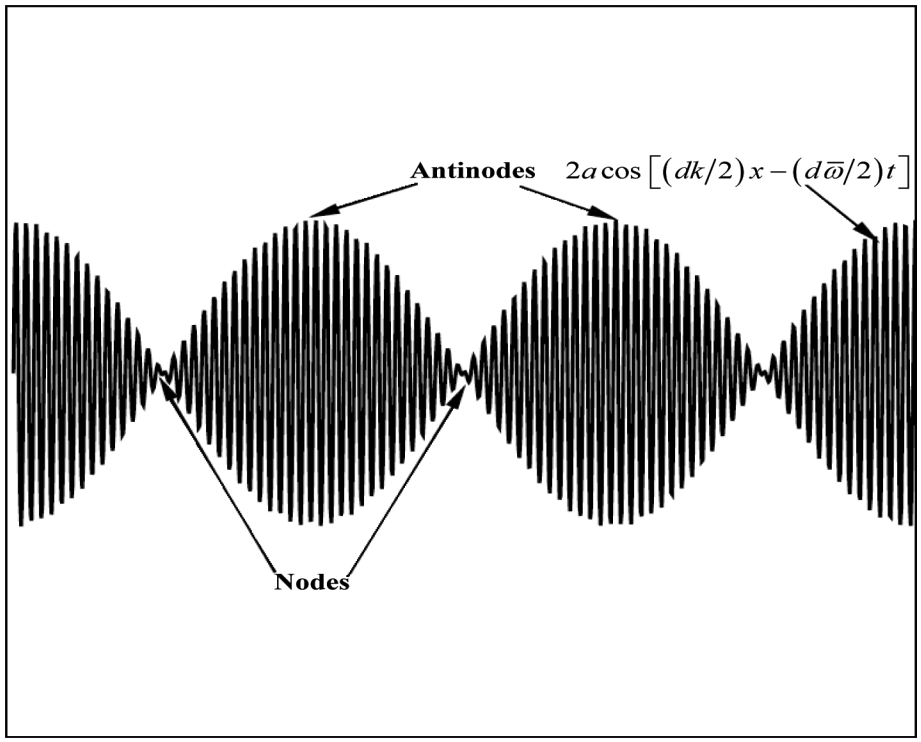

FIGURE 2.14

Schematic of the energy spectrum in Kolmogorov's theory is shown at the top. The dissipation spectrum as used in Kolmogorov's theory is shown at the bottom.

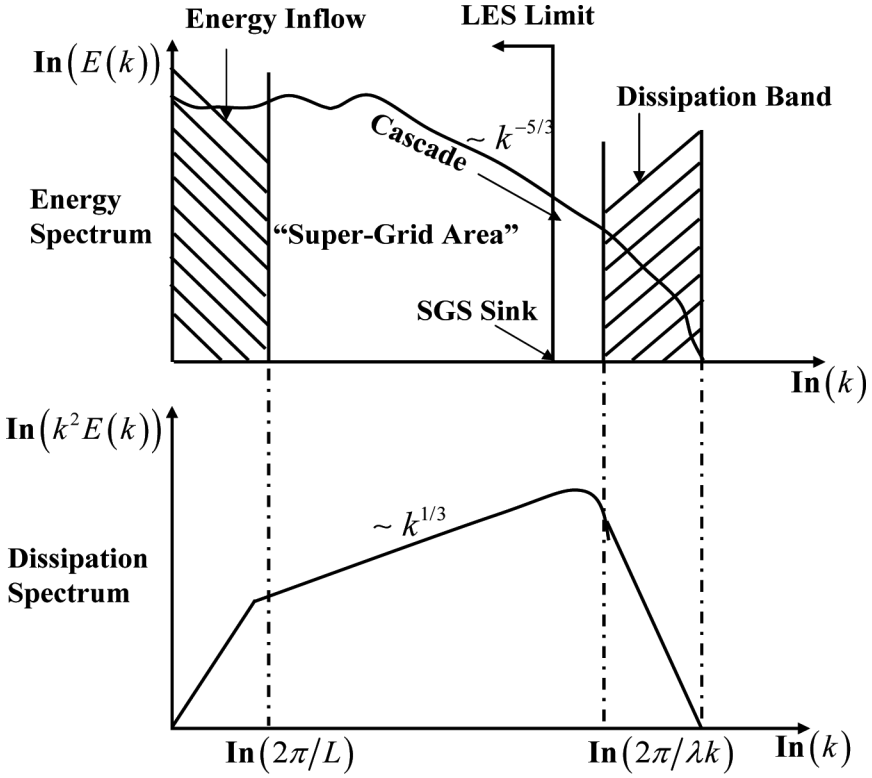

FIGURE 2.15

Sketch of the turbulent flow energy spectrum, exhibiting both two-dimensional and threedimensional flow natures, as drawn in some monographs, showing energy and enstrophy cascades. (Reproduced with permission from Doering and Gibbon, *Applied Analysis of the Navier–Stokes Equations*, Copyright (1995) Cambridge University Press.)

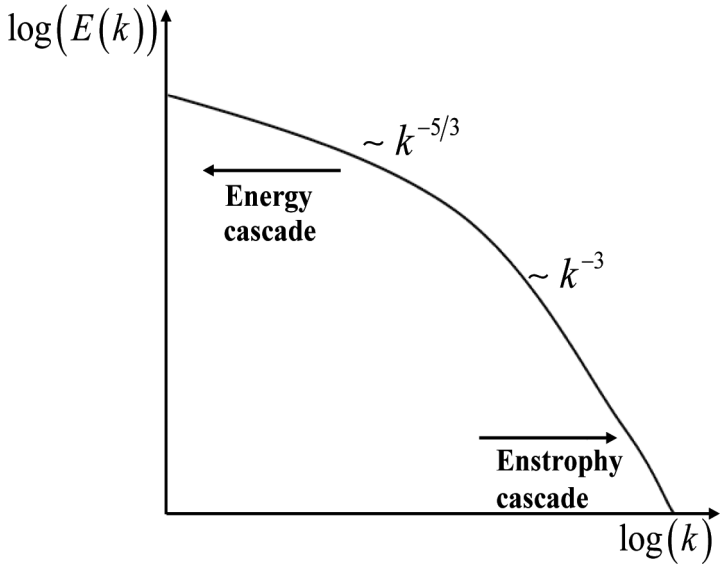

FIGURE 2.16

Power spectra of wind and potential temperature in the atmosphere measured at tropopause by an aircraft (data taken from [244]). (Reproduced with permission from Galperin and Orszag, *Large Eddy Simulation of Complex Engineering and Geophysical Flows*, Copyright (1993) Cambridge University Press.)

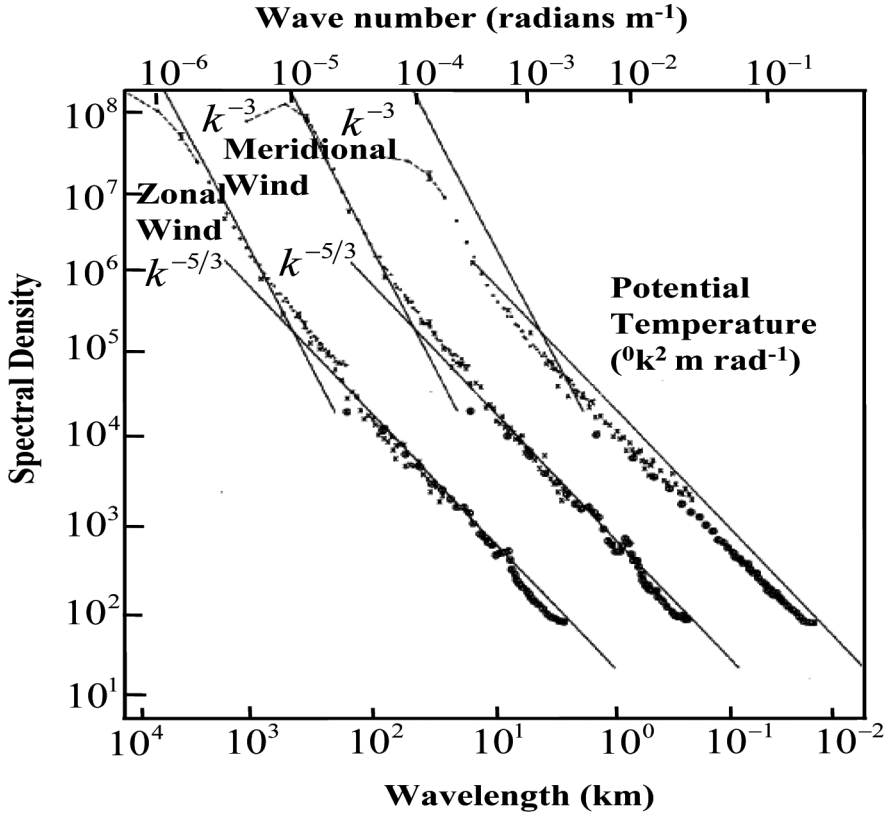

FIGURE 2.17

Ranges of temporal scales excited in flows of engineering interest for different speeds and the corresponding frequency ranges (Ω_f). Also, indicated is the band for mean frequencies of large eddies in high Reynolds number flows.

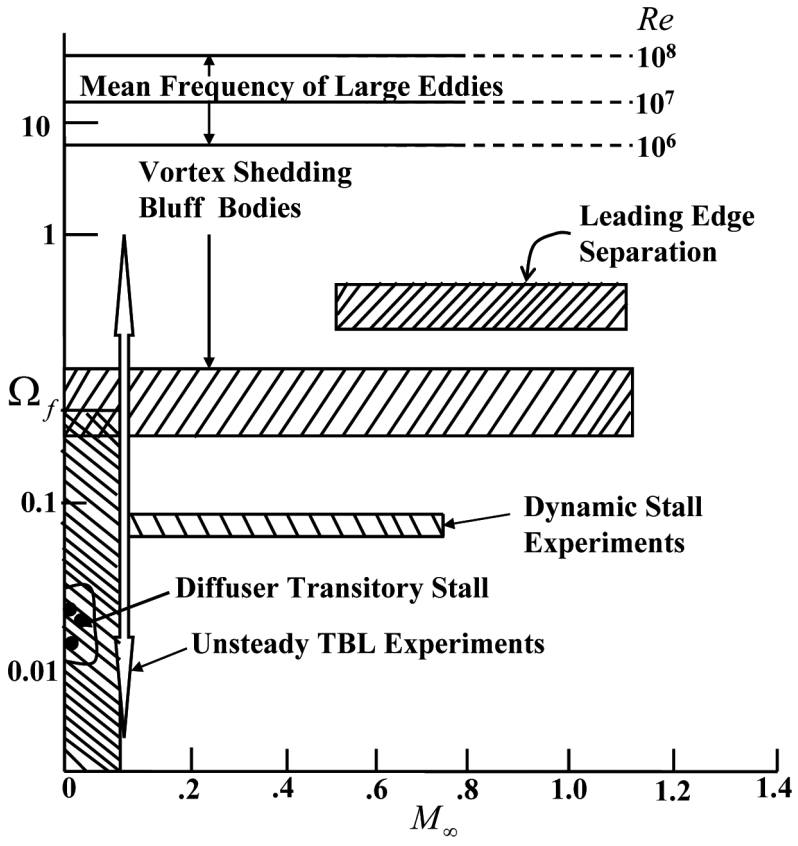

FIGURE 2.18

Comparison of numerical amplification factor ($|G|$), normalized numerical group velocity (V_{gN}/c) and phase error ($1 - c_N/c$) contours for the near-boundary node $j = 2$ (left column) and central node $j = 51$ (right column) for the 1D convection equation solved by the OUCS3-RK_4 method.

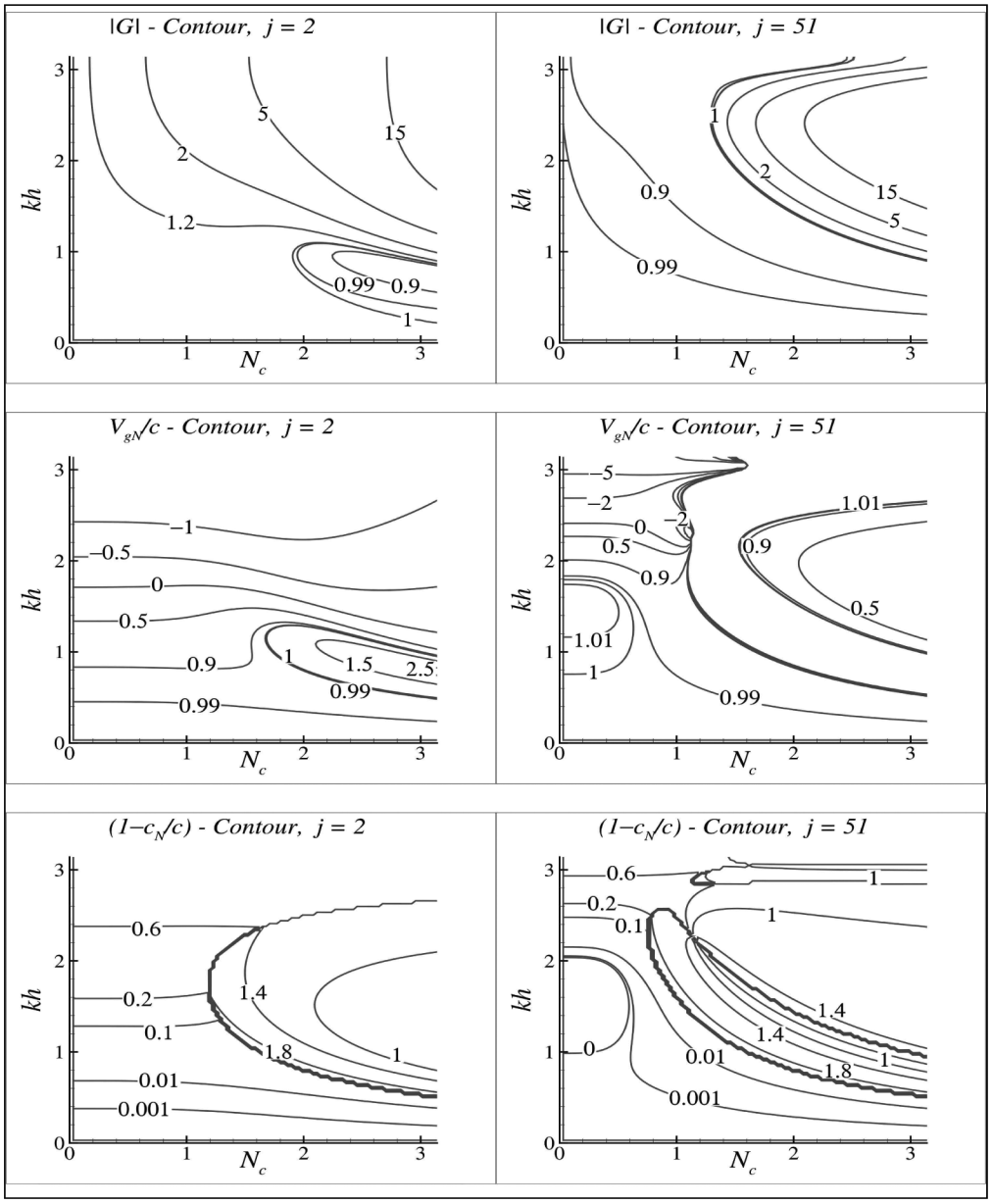

FIGURE 2.19

Comparison of the numerical amplification factor (|*G*|) for interior nodes by the indicated combinations of space–time discretization schemes.

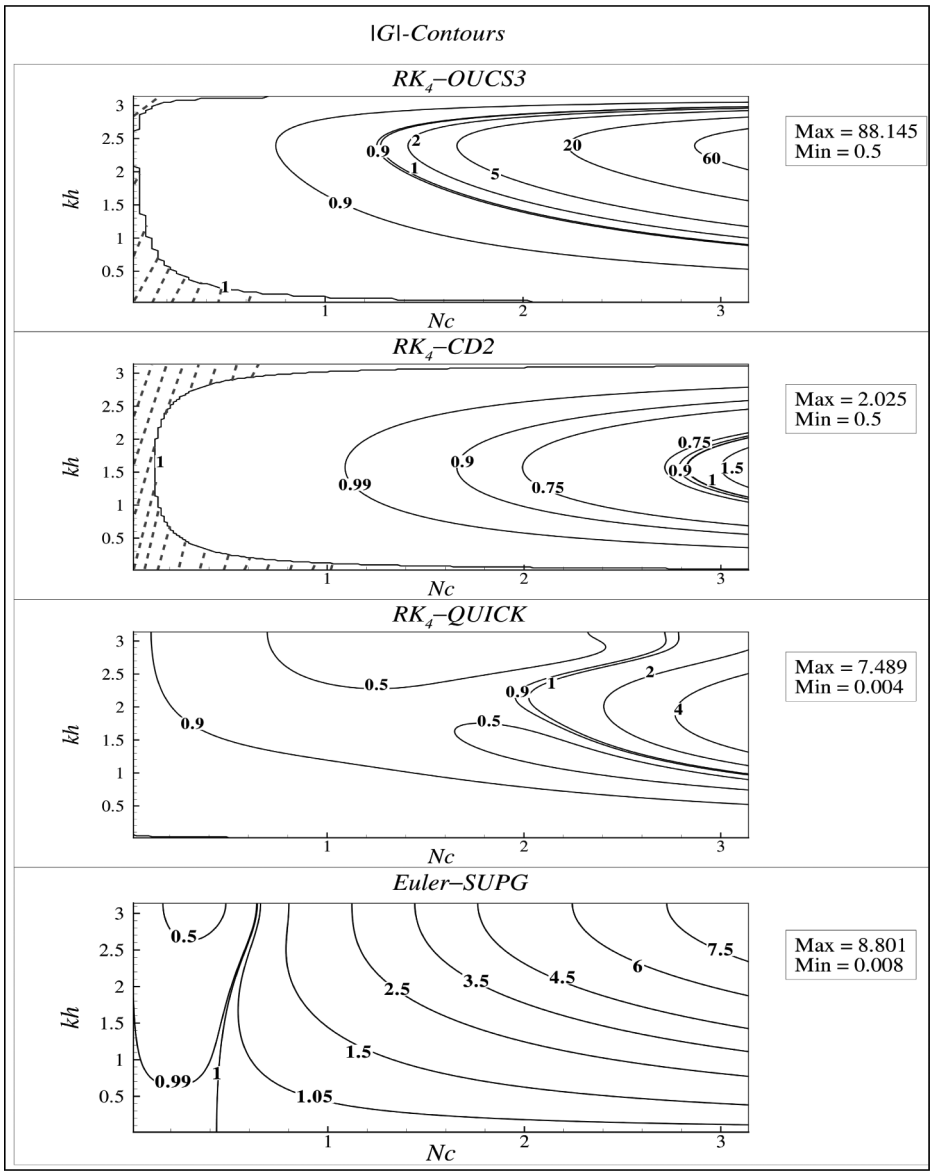

FIGURE 2.20

Comparison of normalized numerical group velocity (V_{gN}/c) for interior nodes for the indicated combinations of space–time discretizations.